

# Some Microstructural Properties of Zinc Borosilicate Glass as a Possible Matrix in the Immobilization of Various Wastes

Svetozar Musić,<sup>1,2,\*</sup> Marijan Marciuš,<sup>1</sup> Stjepko Krehula,<sup>1</sup> Stanko Popović,<sup>2,3</sup>  
 Ernő Kuzmann,<sup>4</sup> Zoltán Homonnay<sup>4</sup>

<sup>1</sup> Ruđer Bošković Institute, Bijenička cesta 54, HR-10000 Zagreb, Croatia

<sup>2</sup> Croatian Academy of Sciences and Arts, Trg Nikole Šubića Zrinskog 11, HR-10000 Zagreb, Croatia

<sup>3</sup> Department of Physics, Faculty of Science, University of Zagreb, Bijenička cesta 32, HR-10000 Zagreb, Croatia

<sup>4</sup> Institute of Chemistry, Eötvös Loránd University, Budapest, Hungary

\* Corresponding author's e-mail address: music@irb.hr

RECEIVED: September 24, 2019 \* REVISED: October 18, 2019 \* ACCEPTED: October 20, 2019

**Abstract:** Zinc borosilicate glass with optimized chemical composition was synthesized and doped with 5 wt %  $\alpha$ -Fe<sub>2</sub>O<sub>3</sub>. XRD, <sup>57</sup>Fe Mössbauer, FT-IR, UV/Vis/NIR and FE SEM were used as the characterization methods. XRD showed the amorphous nature of the samples synthesized. <sup>57</sup>Fe Mössbauer spectra confirmed the superposition of Fe<sup>3+</sup> in tetrahedral and Fe<sup>2+</sup> in octahedral positions. FT-IR spectra showed general features characteristic of different borosilicate glasses. The NIR band at 1116 nm in the UV/Vis/NIR spectrum was assigned to the Fe<sup>2+</sup> transition, whereas the Fe<sup>3+</sup> transition bands could not be assigned due to the overlapping of several spectral bands of different origin in the UV region centered at 282 nm and the Vis region between 415 to 496 nm. Zinc borosilicate glass as synthesized can be considered as a possible matrix in the immobilization of nonradioactive as well as radioactive wastes.

**Keywords:** zinc borosilicate glass, immobilization matrix, nonradioactive waste, radioactive waste, XRD, <sup>57</sup>Fe Mössbauer, FT-IR, UV/Vis/NIR.

## INTRODUCTION

VARIOUS wastes (nonradioactive and radioactive) generated by man's activity are creating great problems in the contemporary world, and for this reason it is not surprising that many scientists and engineers are searching for the methods of their immobilization. Nonradioactive waste can be of different origins, for example, generated by the incineration of municipal, medical or biomass waste, the combustion of coal in thermal power plants as well as from slag in iron metallurgy, mud from metal in hydrometallurgy, etc. Glass and glass-ceramics have been considered for the immobilization of nonradioactive waste<sup>[1–5]</sup> with further application as ceramics and construction materials. Radioactive waste can be produced in different steps of the nuclear fuel cycle or during the application of radioisotopes to other human activities. Glass-forming regions in the

system ZnO–B<sub>2</sub>O<sub>3</sub>–SiO<sub>2</sub><sup>[6]</sup> as well as the effects of the ZnO component in the borosilicate glass matrix on a possible immobilization of radioactive waste were investigated.<sup>[7–10]</sup>

In this paper we present some microstructural properties of zinc borosilicate glass with optimized chemical composition for a possible immobilization of nonradioactive or radioactive wastes.

## EXPERIMENTAL

### Preparation of Glass Samples

Zinc borosilicate glass was prepared using the commercial chemicals, ZnO, H<sub>3</sub>BO<sub>3</sub>, Na<sub>2</sub>CO<sub>3</sub>, K<sub>2</sub>CO<sub>3</sub>, CaCO<sub>3</sub>, MgO, SrCO<sub>3</sub>, BaCO<sub>3</sub>, whereas amorphous SiO<sub>2</sub> was prepared by Musić et al.<sup>[11]</sup> The starting chemical composition (in wt %) of zinc borosilicate glass in the form of oxide was the following: 28.8 % ZnO, 15.2 % B<sub>2</sub>O<sub>3</sub>, 37.0 % SiO<sub>2</sub>, 5.5 % Na<sub>2</sub>O, 5.5 % K<sub>2</sub>O,

2.0 % CaO, 2.0 % MgO, 2.0 % SrO and 2.0 % BaO. The iron component was added in the form of hematite (5 wt %  $\alpha$ -Fe<sub>2</sub>O<sub>3</sub>) powder supplied by *Ventron*.

The corresponding amounts of the chemicals were mixed with a small amount of twice distilled water, then dried. After drying this mixture was ground, then melted in ceramic crucible in a laboratory furnace while gradually increasing temperature up to 1000 °C and kept at this temperature for 4h. In the case of the zinc borosilicate glass matrix loaded with 30 wt %  $\alpha$ -Fe<sub>2</sub>O<sub>3</sub> the system was additionally heated to 1100 °C for 1 h. Molten glass was poured into a preheated graphite mould, then cooled to room temperature.

### Instrumentation

XRD patterns were recorded at 20 °C with an APD 2000 diffractometer manufactured by *ItalStructures* (Novara, Italy).

Mössbauer spectra were recorded at 295 and 80 K in the transmission mode using the instrumentation by *WissEl* (Starnberg, Germany). A <sup>57</sup>Co/Rh Mössbauer source was used. The velocity scale and all Mössbauer data refer to the  $\alpha$ -Fe absorber at 295 K. Mössbauer spectra were evaluated using the *MossWinn* program.

FT-IR spectra were recorded at RT using a *Perkin-Elmer* spectrometer (model *Frontier*).

UV/Vis/NIR spectra were recorded at RT using a UV-3600 spectrometer manufactured by *Shimadzu* and equipped with an integrating sphere. Extra pure BaSO<sub>4</sub> by *Wako* Chemicals was used as a reference.

FE SEM images were taken with a thermal field emission scanning electron microscope (model JSM 7000F) manufactured by *JEOL* Ltd.

## RESULTS AND DISCUSSION

Figure 1. shows the XRD patterns of (a) zinc borosilicate glass, and (b) with 5 wt % loading of  $\alpha$ -Fe<sub>2</sub>O<sub>3</sub>. These XRD patterns did not show any presence of a crystalline phase. Figure 2 shows the Mössbauer spectra of zinc borosilicate glass containing iron ions. These spectra, as recorded at 295 and 80 K, indicate the superposition of two quadrupole doublets with Mössbauer parameters given in Table 1. The doublet with a greater quadrupole splitting can be assigned to Fe<sup>2+</sup> ions in the octahedral environment, whereas the one with a lower quadrupole splitting can be assigned to Fe<sup>3+</sup> ions in the tetrahedral environment. Cochain et al.<sup>[12]</sup> reported about the state of iron in silicate glasses. In these glasses Fe<sup>2+</sup> is present in octahedral and Fe<sup>3+</sup> in tetrahedral coordination. A similar conclusion was reached by Taragin and Eisenstein<sup>[13]</sup> for the state of iron in some borosilicate glasses. Romero et al.<sup>[14,15]</sup> investigated the state of iron in borosilicate glasses of different chemical composition and

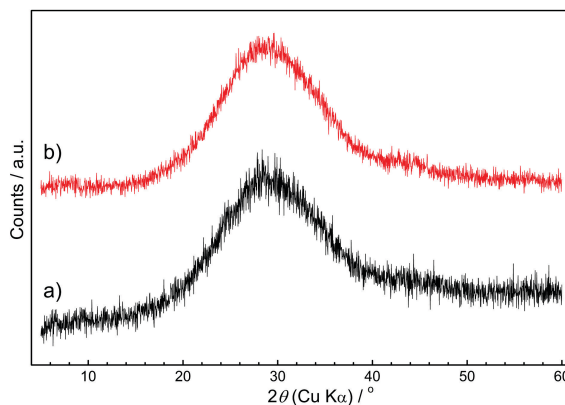


**Figure 1.** XRD patterns of (a) zinc borosilicate glass, and (b) with 5 wt % loading of  $\alpha$ -Fe<sub>2</sub>O<sub>3</sub>.

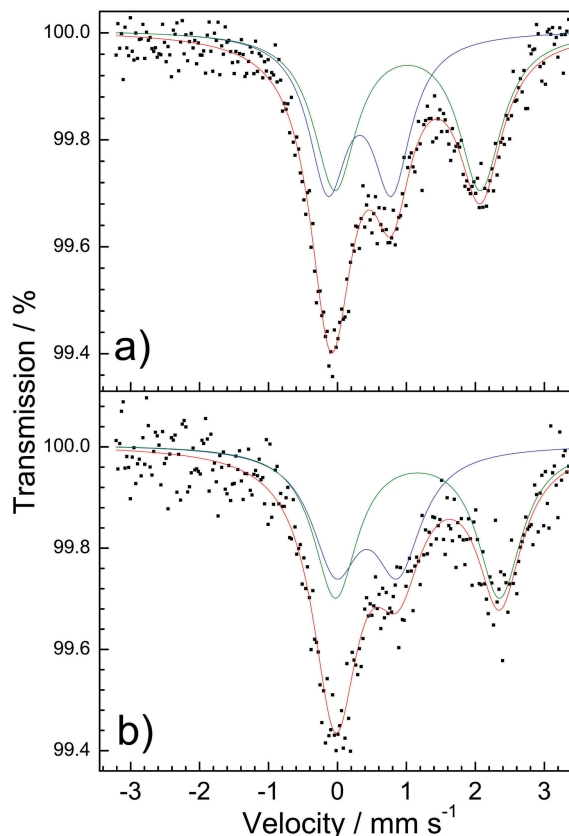


**Figure 2.** <sup>57</sup>Fe Mössbauer spectra of zinc borosilicate glass containing dissolved iron ions as recorded at (a) 295 K and (b) 80 K.

found a dependence of the Fe<sup>3+</sup>/Fe<sup>2+</sup> ratio on the Fe<sub>2</sub>O<sub>3</sub> content as well as an increasing distortion of the glass network with the increased Fe<sub>2</sub>O<sub>3</sub> content. Table 1 shows a significant broadening of quadrupole splitting lines which can be assigned to a wide distribution of iron at Fe<sup>2+</sup> and Fe<sup>3+</sup> sites in the amorphous glass matrix. Generally, it is

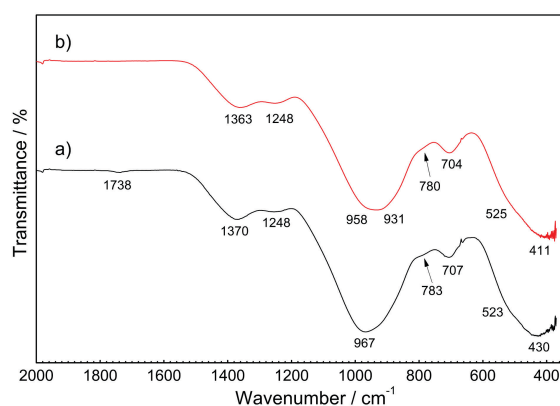
**Table 1.**  $^{57}\text{Fe}$  Mössbauer parameters of zinc borosilicate glass doped with 5 wt %  $\alpha\text{-Fe}_2\text{O}_3$ .

Line	$\delta / \text{mm s}^{-1}$	$\Delta / \text{mm s}^{-1}$	$\Gamma / \text{mm s}^{-1}$	Area / %	$T / \text{K}$
Q <sub>1</sub>	0.32	0.92	0.68	46.3	295
Q <sub>2</sub>	1.02	2.11	0.76	53.7	295
Q <sub>1</sub>	0.42	0.90	0.83	45.0	80
Q <sub>2</sub>	1.16	2.38	0.78	55.0	80

Key:  $\delta$  = isomer shift;  $\Delta$  = quadrupole splitting;  $\Gamma$  = line width  
Errors:  $\delta = \pm 0.01 \text{ mm s}^{-1}$ ;  $\Delta = \pm 0.01 \text{ mm s}^{-1}$ .

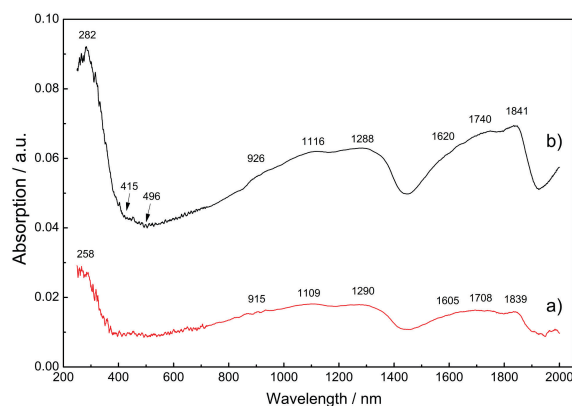
argued that the incorporation of iron ions in the borosilicate matrix reduces the boron coordination that is demonstrated by a decrease in the amount of  $\text{BO}_4$  tetrahedra and a corresponding increase in  $\text{BO}_3$  triangles. This is accompanied by the breaking of Si–O–B network bonds and the formation of Si–O– $\text{Fe}^{3+}$  bridge bonds as well as Si–O<sup>-</sup> nonbridging bonds including  $\text{Fe}^{2+}$  as modifying cations.<sup>[16,17]</sup>

The FT-IR spectra of (a) zinc borosilicate glass, and (b) with 5 wt % loading of  $\alpha\text{-Fe}_2\text{O}_3$  are shown in Figure 3. General features of these spectra are typical of borosilicate glass. The weak IR band at  $1738 \text{ cm}^{-1}$  (Figure 3a) can be assigned to the ring asymmetric stretching relaxation of B–O bonds in  $\text{BO}_3$  triangles. The IR band at  $1370 \text{ cm}^{-1}$  can be related to the ring stretching vibrations of  $\text{BO}_3$  whereas the IR band at  $1248 \text{ cm}^{-1}$  is usually interpreted as the bond stretching vibration of the boron sublattice against the oxygen sublattice. A very strong IR band centered at  $967 \text{ cm}^{-1}$  can be assigned to the stretching vibrations of Si–O and B–O bonds of tetrahedrally coordinated  $\text{Si}^{4+}$  and  $\text{B}^{3+}$ . This IR band showed a very high broadening, thus indicating that there is a superposition of several IR bands. The IR band at  $707$  to  $704 \text{ cm}^{-1}$  can be related to the vibrations of the B–O bond in a  $\text{BO}_3$  triangle with an increased relative

**Figure 3.** FT-IR spectra of (a) zinc borosilicate glass, and (b) with 5 wt % loading of  $\alpha\text{-Fe}_2\text{O}_3$ .

intensity of this band while increasing  $\alpha\text{-Fe}_2\text{O}_3$  or waste loadings. Finally, a very strong and broadened IR band at  $430 \text{ cm}^{-1}$  was observed, which could be assigned to the bending vibrations within  $\text{SiO}_4$  tetrahedra (O–Si–O) and between  $\text{SiO}_4$  tetrahedra (Si–O–Si) as well as the Zn vibrations within  $\text{ZnO}_6$  octahedra and other Me–O bonds (Me–Mg, Ca, Sr, Ba). The addition of 5 wt %  $\alpha\text{-Fe}_2\text{O}_3$  to the zinc borosilicate glass matrix did not significantly influence the corresponding FT-IR spectrum (Figure 3b). More about the interpretations of the borosilicate glass structure based on infrared spectroscopy can be found in reference literature.<sup>[18–22]</sup>

Figure 4. shows the UV/Vis/NIR spectra of (a) zinc borosilicate glass, and (b) with 5 wt % loading of  $\alpha\text{-Fe}_2\text{O}_3$ . Here it can be mentioned that the UV/Vis/NIR spectra of borosilicate glasses were much less investigated than the infrared spectra of the same glasses. Kukkadapu et al.<sup>[23]</sup> investigated sodium silicate glass doped with 0.5 mol %  $\text{Fe}_2\text{O}_3$ . The broad bands at 1120 and 2020 nm were assigned to the  $\text{Fe}^{2+}$  transition, whereas the minor bands at 375, 415 and 435 nm as well as the broad band at  $\sim 485 \text{ nm}$  were assigned to the  $\text{Fe}^{3+}$  transition. In the present UV/Vis/NIR spectrum (Figure 4.b) the band at 1116 nm is visible as a shoulder. Moreover, in the same spectral region two shoulders at 926 and 1288 nm are also visible. However, in the present case there are no great differences between the UV/Vis/NIR spectra of undoped and Fe-doped zinc borosilicate glasses. El Batal et al.<sup>[24]</sup> investigated the UV/Vis spectra of TM-doped  $\text{Na}_2\text{O–B}_2\text{O}_3\text{–SiO}_2$  glasses (TM = transition metal). The spectrum of Fe-doped sodium borosilicate glass showed four prominent UV bands at 210, 235, 275 and 315 nm as well as two weak bands at 380 and 440 nm. The increase in relative intensity with progressive gamma irradiation was explained by the oxidation of  $\text{Fe}^{2+}$  and the formation of  $\text{Fe}^{3+}$ . Bartoll et al.<sup>[25]</sup> found a band at 300 nm in the UV/Vis spectrum of gamma irradiated Fe-doped alkaline earth silicate glasses. In the present case Fe-

**Figure 4.** UV/Vis/NIR spectra of (a) zinc borosilicate glass, and (b) with 5 wt % loading of  $\alpha\text{-Fe}_2\text{O}_3$ .

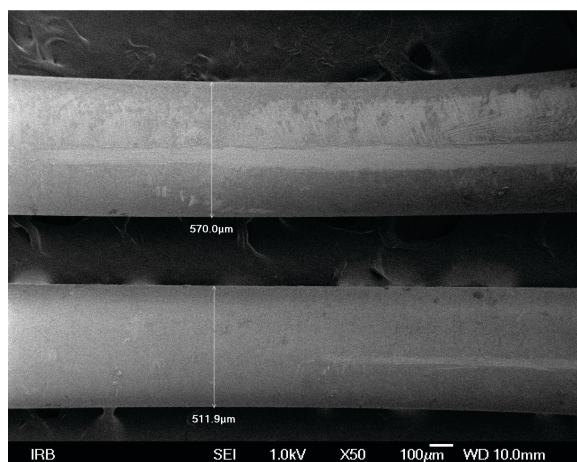


**Figure 5.** Zinc borosilicate glass fibers loaded with 5 wt % of  $\alpha\text{-Fe}_2\text{O}_3$  as withdrawn from the melt.

doped zinc borosilicate glass showed a very strong and broad band centered at 282 nm. A very weak shoulder at 415 to 496 nm was also visible due to the presence of  $\text{Fe}^{3+}$  ions.

The zinc borosilicate glass matrix as described has a high loading capacity for various wastes. However, when the waste loading was simulated with 30 wt %  $\alpha\text{-Fe}_2\text{O}_3$ , the XRD pattern showed the crystallization of the spinel phase ( $\sim 10\%$ ) inside the glass matrix. Furthermore, glass fibers (or glass wool) can be produced by drawing out from molten zinc borosilicate glass. Figure 5. shows glass fibers obtained from the zinc borosilicate glass matrix loaded with 5 wt %  $\alpha\text{-Fe}_2\text{O}_3$ . In the case of nonradioactive waste, due to economic reasons, strontium can be replaced with cheaper alkaline earths.

## CONCLUSIONS

Zinc borosilicate glass with optimized chemical composition was synthesized and showed a completely amorphous nature. Upon loading with 5 wt %  $\alpha\text{-Fe}_2\text{O}_3$  the Mössbauer spectra at 295 and 80 K showed a superposition of two quadrupole doublets corresponding to  $\text{Fe}^{3+}$  in tetrahedral positions and  $\text{Fe}^{2+}$  in octahedral positions. The ratio  $\text{Fe}^{3+}/\text{Fe}^{2+} = 0.86$  was measured at 295 K and a similar ratio was obtained at 80 K. The FT-IR spectra showed the general features of the borosilicate glass matrix. In the UV/Vis/NIR spectrum the NIR band at 1116 nm was assigned to  $\text{Fe}^{2+}$  ions, whereas in the UV/Vis/NIR region the  $\text{Fe}^{3+}$  transitions were not well visible due to the overlapping of several UV bands centered at 282 nm and several Vis bands between 415 and 496 nm. The zinc borosilicate glass matrix can be considered in the immobilization of nonradioactive or radioactive wastes.

**Acknowledgment.** The authors wish to thank Marijan Gotić for his assistance in the investigation of zinc borosilicate glass.

## REFERENCES

- [1] J. Ma. Rincón, M. Romero, A. R. Boccaccini, *J. Mater. Sci.* **1999**, *34*, 4413–4423. <https://doi.org/10.1023/A:1004620818001>
- [2] R. D. Rawlings, J. P. Wu, A. R. Boccaccini, *J. Mater. Sci.* **2006**, *41*, 733–761. <https://doi.org/10.1007/s10853-006-6554-3>
- [3] S. R. Teixeira, R. S. Magalhães, A. Arenales, A. E. Souza, M. Romero, J. Ma. Rincón, *J. Environ. Management*, **2014**, *134*, 15–19. <https://doi.org/10.1016/j.jenvman.2013.12.029>
- [4] M. Romero, M. S. Hernández-Crespo, J. Ma. Rincón, *Adv. Appl. Ceramics* **2009**, *108*, 67–71. <https://doi.org/10.1179/174367608X366337>
- [5] S. Ballesteros, J. Ma. Rincón, B. Rincón-Mora, M. M. Jordán, *J. Geochem. Exploration* **2017**, *174*, 132–139. <https://doi.org/10.1016/j.gexplo.2016.07.011>
- [6] E. H. Hamilton, R. M. Waxler, J. M. Nivert Jr., *J. Res. Nat. Bureau Stand.* **1959**, *62*, 59–62. <https://doi.org/10.6028/jres.062.011>
- [7] D. E. Clark, E. L. Yen-Bower, L. L. Hench, Corrosion Behavior of Zinc Borosilicate Simulated Nuclear Waste Glass, *Cearmics in Nuc. Waste Manage., Proc. of Int. Symp. Cincinnati*, OH, 30 April – 2 May **1979**, 256–262.
- [8] H. Zhang, C. L. Corkhill, P. G. Heath, R. J. Hand, M. C. Stennett, N. C. Hyatt, *J. Nucl. Mater.* **2015**, *462*, 321–328. <https://doi.org/10.1016/j.jnucmat.2015.04.016>
- [9] N. J. Cassingham, C. L. Corkhill, M. C. Stennett, R. J. Hand, N. C. Hyatt, *J. Nucl. Mater.* **2016**, *479*, 639–646. <https://doi.org/10.1016/j.jnucmat.2016.06.009>
- [10] S. Musić, M. Gotić, S. Popović, B. Gržeta, *J. Radioanal. Nucl. Chem.* **1987**, *116*, 141–157. <https://doi.org/10.1007/BF02037218>
- [11] S. Musić, N. Filipović-Vinceković, L. Sekovanić, *Braz. J. Chem. Eng.* **2011**, *28*, 89–94. <https://doi.org/10.1590/S0104-66322011000100011>
- [12] B. Cochain, D. R. Neuville, G. S. Henderson, C. A. McCammon, O. Pinet, P. Richet, *J. Am. Ceram. Soc.* **2012**, *95*, 962–971.
- [13] M. F. Taragin, J. C. Eisenstein, *J. Non-Crystalline Solids* **1970**, *3*, 311–316. [https://doi.org/10.1016/0022-3093\(70\)90001-3](https://doi.org/10.1016/0022-3093(70)90001-3)
- [14] M. Romero, J. Ma. Rincón, S. Musić, V. Kozhukharov, *Mater. Res. Bull.* **1999**, *34*, 1107–1115. [https://doi.org/10.1016/S0025-5408\(99\)00110-5](https://doi.org/10.1016/S0025-5408(99)00110-5)
- [15] M. Romero, J. Ma. Rincón, S. Musić, V. Kozhukharov, *Revista de Metalurgia (Madrid)*, **1997**, *33*, 317–323. <https://doi.org/10.3989/revmetalm.1997.v33.i5.844>

- [16] V. E. Eremyashev, A. B. Mironov, *Inorg. Mater.* **2015**, *51*, 177–181.  
<https://doi.org/10.1134/S0020168515020065>
- [17] Y. S. Glazkova, S. N. Kalmykov, I. A. Presnyakov, O. I. Stefanovskaya, S. V. Stefanovsky, *Glass Phys. Chem.* **2015**, *41*, 367–377.  
<https://doi.org/10.1134/S1087659615040057>
- [18] A. S. Tenney, J. Wong, *J. Chem. Phys.* **1972**, *56*, 5516–5523.  
<https://doi.org/10.1063/1.1677069>
- [19] Y. Sun, Z. Zhang, *Metall. Mater. Trans. B*, **2015**, *46*, 1549–1554.  
<https://doi.org/10.1007/s11663-015-0374-2>
- [20] M. S. Meikhail, A. M. Abdelghany, *Silicon*, **2017**, *9*, 895–900. <https://doi.org/10.1007/s12633-016-9543-4>
- [21] H. Kamal, A. M. Hezma, *Silicon*, **2018**, *10*, 851–858.  
<https://doi.org/10.1007/s12633-016-9540-7>
- [22] A. Madheshiya, K. K. Dey, M. Ghosh, J. Singh, C. Gautam, *J. Non-Crystalline Solids* **2019**, *503–504*, 288–296.  
<https://doi.org/10.1016/j.jnoncrysol.2018.10.009>
- [23] R. K. Kukkadapu, H. Li, G.L. Smith, J. D. Crum, J.-S. Jeoung, W. H. Poisl, M. C. Weinberg, *J. Non-Crystalline Solids* **2003**, *317*, 301–318.  
[https://doi.org/10.1016/S0022-3093\(02\)01815-X](https://doi.org/10.1016/S0022-3093(02)01815-X)
- [24] F. H. El Batal, M. S. Selim, S. Y. Marzouk, M. A. Azooz, *Physica B* **2007**, *398*, 126–134.  
<https://doi.org/10.1016/j.physb.2007.05.004>
- [25] J. Bartoll, M. Nofz, R. Stösser, *Phys. Chem. Glasses* **2000**, *41*, 140–149.